JACS
JOURNAL OF THE AMERICAN CHEMICAL SOCIETY

COMMUNICATION

pubs.acs.org/JACS

Nanoporous Graphitic-C_3N_4@Carbon Metal-Free Electrocatalysts for Highly Efficient Oxygen Reduction

Yao Zheng,[†] Yan Jiao,[‡,§] Jun Chen,[∥] Jian Liu,[†] Ji Liang,[†] Aijun Du,[‡] Weimin Zhang,[∥] Zhonghua Zhu,[§] Sean C. Smith,[‡] Mietek Jaroniec,[⊥] Gao Qing (Max) Lu,[†] and Shi Zhang Qiao*[,†]

[†]ARC Centre of Excellence for Functional Nanomaterials, Australian Institute for Bioengineering and Nanotechnology, The University of Queensland, QLD 4072 Brisbane, Australia

[‡]Centre for Computational Molecular Science, Australian Institute for Bioengineering and Nanotechnology, The University of Queensland, QLD 4072 Brisbane, Australia

[§]School of Chemical Engineering, The University of Queensland, QLD 4072 Brisbane, Australia

[∥]Intelligent Polymer Research Institute, ARC Centre of Excellence for Electromaterials Science, Australian Institute of Innovative Materials, University of Wollongong, NSW 2522, Australia

[⊥]Department of Chemistry, Kent State University, Kent, Ohio 44242, United States

Supporting Information

ABSTRACT: Based on theoretical prediction, a g-C_3N_4@carbon metal-free oxygen reduction reaction (ORR) electrocatalyst was designed and synthesized by uniform incorporation of g-C_3N_4 into a mesoporous carbon to enhance the electron transfer efficiency of g-C_3N_4. The resulting g-C_3N_4@carbon composite exhibited competitive catalytic activity (11.3 mA cm^{-2} kinetic-limiting current density at −0.6 V) and superior methanol tolerance compared to a commercial Pt/C catalyst. Furthermore, it demonstrated significantly higher catalytic efficiency (nearly 100% of four-electron ORR process selectivity) than a Pt/C catalyst. The proposed synthesis route is facile and low-cost, providing a feasible method for the development of highly efficient electrocatalysts.

The sluggish kinetics of the cathodic oxygen reduction reaction (ORR) significantly limits the efficiency and performance of electrochemical energy conversion in fuel cells.[1] Although precious Pt has been adopted as an effective ORR electrocatalyst, large-scale commercial production has been restricted by its prohibitive cost, limited supply, and weak durability. The state-of-the-art metal-free nitrogen-doped carbon (N-carbon) materials are generally accepted as a potential substitute for Pt to reduce the cost, enhance the stability of ORR electrocatalysts, and then promote the commercialization of fuel cell technology.[1c,2] Nitrogen doping can enhance the electron-donor property of the carbon matrix, resulting in an improvement of the interaction between carbon and guest molecules.[1c,2a] However, several issues still exist with N-carbon materials including whether the catalytic activity is caused by its unique electronic properties or metal residue from its metal-involved synthesis process.[2] In addition, the relatively low nitrogen content (2−5%) and a leaching of nitrogen active sites result in low and unstable catalytic activity of N-carbon materials. To this end, the development of a completely metal-free ORR electrocatalyst with high nitrogen content and a stable structure is highly desirable for elucidation of the correlation between the structure, composition, and electrochemical activity of these promising materials.[3]

Graphitic-carbon nitride, referred to as g-C_3N_4, can be synthesized from a simple precursor via a series of polycondensation reactions without any metal involvement.[4a] g-C_3N_4 shows remarkably high catalytic activity for a variety of reactions such as photocatalytic hydrogen production.[4] Because of its high nitrogen content and facile synthesis procedure, g-C_3N_4 may provide more active reaction sites than other N-carbon materials to serve as a feasible metal-free ORR electrocatalyst.[5a] However, reports on the application of g-C_3N_4 in fuel cells and other electrochemical applications are rare and no theoretical calculation has been done to predict its unexplored electrocatalytic capacity.[5b,c]

Herein we theoretically clarify the major barrier of ORR on g-C_3N_4 by first-principle calculations and evaluate its potential as an efficient ORR electrocatalyst. The results indicate that the limited electron transfer (ET) ability of g-C_3N_4 is conducive for the accumulation of OOH^- intermediate products via an inefficient two-electron ($2e^-$) ORR pathway, one of the main reasons for its relatively low ORR catalytic activity. Based on this theoretical prediction, our proof-of-concept studies were carried out by incorporating the g-C_3N_4 catalyst into the framework of a highly ordered mesoporous carbon as a g-C_3N_4@carbon to promote ET in the composite and increase the concentration of active sites facilitating ORR. Consequently, the nanoporous g-C_3N_4@carbon showed an excellent electrocatalytic ORR activity and perfect (nearly 100%) four-electron ($4e^-$) ORR pathway selectivity in alkaline aqueous solution. Furthermore, the newly developed catalyst also revealed a remarkable methanol tolerance thus avoiding crossover effects. To the best of our knowledge, such excellent electrochemical performance, which is competitive with a commercial Pt/C catalyst, has been rarely observed for metal-free materials.[5b,d] Therefore, the novel nanoporous g-C_3N_4@carbon with low cost and facile synthesis is a very promising candidate for the next generation of ORR electrocatalysts.

Received: September 29, 2011
Published: November 14, 2011

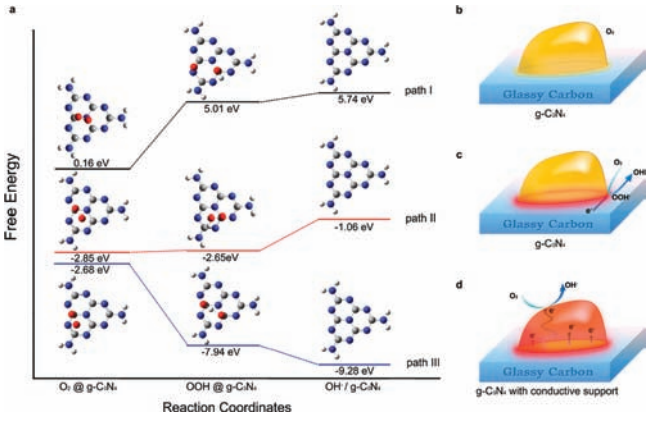

Figure 1. (a) Free energy plots of ORR and optimized configurations of adsorbed species on the g-C_3N_4 surface with zero, two, and four electron participation demonstrated as paths I, II, and III. Energy levels are not drawn to scale. Gray, blue, red, and white small spheres represent C, N, O, and H, respectively. (b–d) Schemes of ORR's pathway on pristine g-C_3N_4 without electron participation, pristine g-C_3N_4 with $2e^-$ participation, and g-C_3N_4 and conductive support composite with $4e^-$ participation, respectively (red areas represent the active sites facilitating ORR).

To understand the fundamental steps of ORR on g-C_3N_4, we carried out first-principle calculations (see Computational Section in Supporting Information for details) based on the standard ORR process in alkaline solutions via either a direct $4e^-$ pathway[6]

$$O_2 + 2H_2O + 4e^- \rightarrow 4OH^- \quad (1)$$

or a two-step $2e^-$ pathway

$$O_2 + H_2O + 2e^- \rightarrow HO_2^- + OH^- \quad (2)$$

$$HO_2^- + H_2O + 2e^- \rightarrow 3OH^- \quad (3)$$

The free energy of each proposed ORR state, including the initial reactant O_2 adsorbed g-C_3N_4 (O_2@g-C_3N_4), intermediate product OOH^- on g-C_3N_4 (OOH@g-C_3N_4), and final product OH^- in the solution with pristine g-C_3N_4 (OH^-/g-C_3N_4), is illustrated in Figure 1a. Paths I, II, and III represent the ORR processes with zero, two, and four electrons participating in the reaction system. As illustrated in path I, oxygen cannot be reduced spontaneously on the pristine g-C_3N_4 surface without electron participation (as shown in Figure 1b) due to the existence of two insurmountable barriers in the free energy plot at the states of intermediate and final products. When a certain amount of electrons is introduced (e.g., two electrons in our calculation, as illustrated in path II), the free energy of intermediate OOH@g-C_3N_4 decreases to a comparable level with that of the initial state of O_2@g-C_3N_4, indicating that the first $2e^-$ reaction (eq 2) can spontaneously proceed. However an obvious barrier still exists at the final state of OH^-/g-C_3N_4, which then blocks the occurrence of the second $2e^-$ reaction (eq 3). As a result, a lot of adsorbed OOH^- intermediate products accumulate on g-C_3N_4, causing a significant ORR resistance. As illustrated in path III, this barrier can be eliminated by introducing more electrons (e.g., four electrons); most of the initially adsorbed O_2 molecules can be quickly reduced to OOH^- and further directly formed OH^- in the solution without any barrier via an efficient $4e^-$ pathway as presented in eq 1. As a result, the OOH^- accumulation as the rate-determining step of ORR with limited electron participation on g-C_3N_4 is successfully eliminated with sufficient electron participation.

The theoretical studies clearly indicate that ORR on g-C_3N_4 can proceed in a more efficient pathway to directly produce the final product with more electron participation. Since g-C_3N_4 is a semiconductor, as illustrated in Figure 1c, the active sites facilitating ORR on g-C_3N_4 are limited to very narrow zones of the electrode–electrolyte–gas three-phase boundaries (TPB) because of the poor ET efficiency, which leads to an unsatisfactory ORR performance. One effective way to increase the number of electrons accumulated on the g-C_3N_4 surface, and then to extend the concentration of active sites, is to add an electron-conductive material as a support for the g-C_3N_4 catalyst. Predictably, as shown in Figure 1d, the active sites facilitating ORR on g-C_3N_4 with a conductive support can spread over the whole surface of the catalyst due to the increased ET efficiency in the composite, which in turn facilitates an efficient $4e^-$ ORR process and sharply enhances the catalyst's performance.

To verify the theoretical prediction, we successfully incorporated g-C_3N_4 into the framework of a highly ordered mesoporous carbon (CMK-3) following a facile nanocasting method. Because of its ordered structure and good electrical conduction, CMK-3 has been widely applied as a conductive support for electrocatalysts in fuel cells and lithium ion batteries.[7a] To uniformly impregnate the g-C_3N_4 layer on the surface of mesoporous carbon, the CMK-3 template was first treated with HNO_3 to introduce hydrophilic groups. After impregnating CMK-3 with the liquid precursor (cyanamide, $CN\text{-}NH_2$) one to three times, the resulting composites were calcined at 550 °C in an inert Ar atmosphere for 4 h to *in situ* synthesize g-C_3N_4 in the voids of the CMK-3 porous framework.

Here we selected g-C_3N_4@CMK-3 obtained by one time precursor impregnation as an example (with 27.1 wt % g-C_3N_4 in the composite). Its ordered mesostructure and high surface area provide a sufficient amount of ORR active sites and facilitate the mass transfer of oxygen molecules (Figures S5, S6). High-resolution transmission electron microscopy (HRTEM) images of the g-C_3N_4@CMK-3 composite (Figure 2a and 2b inset) confirm its highly ordered mesoporous structure. The hexagonal pattern of the *P6mm* symmetrical mesoporous structure can be explicitly observed in Figure 2a, b, indicating a homogeneous distribution of g-C_3N_4 in the framework of CMK-3. The composite exhibits a similar morphology of short nanorods as that of the CMK-3 template with insignificant fraction or aggregation of g-C_3N_4 on the external surface (Figure S7a–c). Electron energy loss spectroscopy (EELS) spectrum and wide-angle X-ray diffraction (XRD) patterns confirm the presence of g-C_3N_4 in the carbon matrix (Figures S7d, S8). In addition, a newly formed C=O bond in g-C_3N_4@CMK-3 can be identified in the X-ray photoelectron spectra (XPS) patterns (Figure S9). This C=O bond facilitates adsorption of the $CN\text{–}NH_2$ precursor in the channels of the CMK-3 template to form a homogeneous structure. It is known that CMK-3 is an assembly of hexagonal arrays of 6–7 nm diameter carbon rods separated by 3–4 nm wide channel voids.[7] As shown in Figure 2c, g-C_3N_4@CMK-3 reveals a similar shape of the nitrogen sorption isotherm (type IV with a distinct hysteresis loop) as CMK-3 (Figure S10c), indicating that the addition of g-C_3N_4 did not cause a significant deterioration of the structure of CMK-3. The obvious decrease in both surface area and pore volume confirms the mesopore filling effect during the impregnation

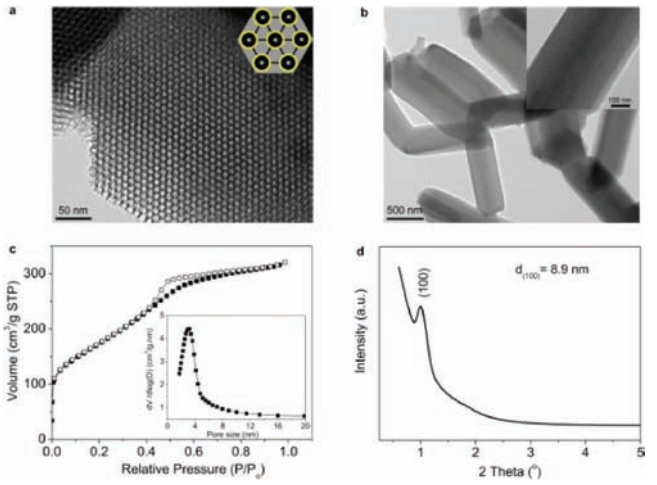

Figure 2. (a,b) Typical HRTEM images of ordered mesoporous g-C_3N_4@CMK-3 nanorods. Inset in panel a represents a schematic illustration (yellow: g-C_3N_4; black: carbon); inset in panel b reveals the ordered mesoporous channels. (c) Nitrogen sorption isotherm at 77 K with the corresponding pore size distribution (inset) and (d) low-angle XRD pattern of g-C_3N_4@CMK-3.

process (Table S4). After impregnation with g-C_3N_4, the original (110) and (200) diffraction peaks on the XRD pattern of CMK-3 almost disappear because of the mesopore filling by g-C_3N_4 (Figures 2d and S10d). The $d_{(100)}$ spacing in both g-C_3N_4@CMK-3 and pristine CMK-3 are ~8.9 nm, indicating the distances between the centers of two carbon nanorods remain unchanged during impregnation (Table S4). The smaller primary pore size of g-C_3N_4@CMK-3 compared to pristine CMK-3 and the narrow pore size distribution (inset of Figure 2c) indicate that the *in situ* synthesized g-C_3N_4 is almost homogeneously distributed on the surface of carbon nanorods, as illustrated by the inset of Figure 2a, resulting in the pore size reduction.

The electrocatalytic activities for ORR on the g-C_3N_4@CMK-3 composite and pristine mesoporous g-C_3N_4 (denoted as g-C_3N_4(m), prepared using mesoporous silica SBA-15 as a sacrificial template (Figure S10)) were first examined by cyclic voltammograms (CVs) in O_2-saturated 0.1 M KOH solution. A physical mixture of CMK-3 and g-C_3N_4(m) (denoted as mixed g-C_3N_4+CMK-3) with identical catalyst content as *in situ* synthesized g-C_3N_4@CMK-3 was also prepared to investigate the possible nanoconfinement phenomena of g-C_3N_4@CMK-3. As shown in Figure 3a, the CV curve recorded for g-C_3N_4@CMK-3 is similar to those obtained on other carbon-based metal-free electrocatalysts with a single ORR peak at −0.25 V.[2b,3,5b−5d,8a−8c] Conversely, there are two obvious ORR peaks at relatively lower cathodic voltage on the CV curves of g-C_3N_4(m) (Figure S11a), corresponding to two separate reduction processes via eqs 2 and 3. It should be noted that the inherent ORR activity on pure CMK-3 is negligible (Figure S11b). Compared with g-C_3N_4(m) and mixed g-C_3N_4+CMK-3, the g-C_3N_4@CMK-3 electrode revealed a more obvious ORR peak with a larger cathodic current, indicating a better electrocatalytic performance for ORR.

A series of linear sweep voltammograms (LSV) on a rotating disk electrode (RDE) further revealed the lower onset potential and higher ORR current density on g-C_3N_4@CMK-3 than g-C_3N_4(m) and mixed g-C_3N_4+CMK-3 electrodes (Figures 3b and S12), consistent with the aforementioned theoretical prediction.

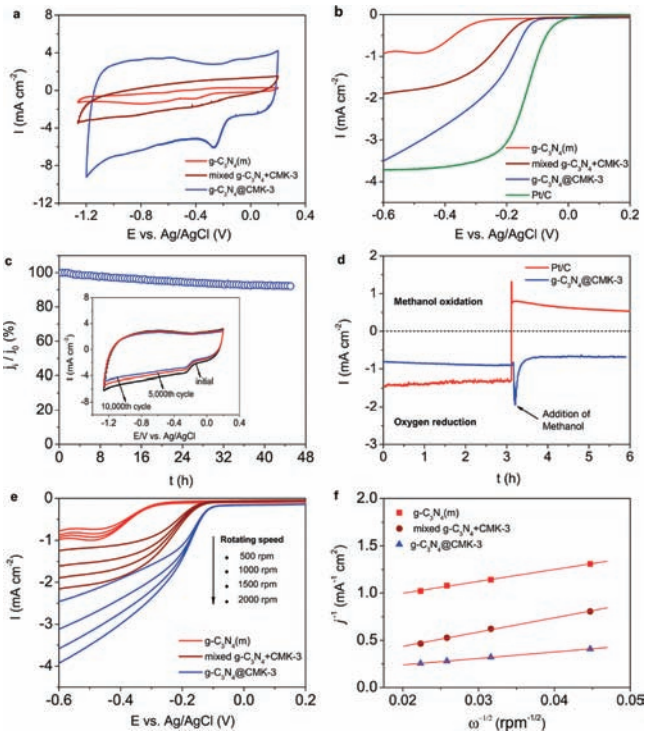

Figure 3. (a) Cyclic voltammograms of ORR on various electrocatalysts in O_2-saturated 0.1 M KOH solution. (b) LSV of various electrocatalysts on RDE at 1500 rpm in O_2-saturated 0.1 M KOH solution. (c) Current−time (i−t) chronoamperometric response of g-C_3N_4@CMK-3 at −0.3 V; inset represents cyclic voltammograms under continuous potentiodynamic sweeps. (d) Chronoamperometric responses of Pt/C and g-C_3N_4@CMK-3 at −0.3 V in O_2-saturated 0.1 M KOH solution without methanol (0−3 h) and with adding methanol (3−6 h). (e,f) LSV of various electrocatalysts on RDE at different rotating rates (500 to 2000 rpm) and corresponding Koutecky−Levich plots at −0.6 V.

Besides, the onset potential on g-C_3N_4@CMK-3 is only ~0.1 V more negative than that on the commercial Pt/C catalyst. At −0.6 V, g-C_3N_4@CMK-3 shows a comparable ORR current density with that observed on Pt/C. It should be noted that the LSV obtained on g-C_3N_4(m) shows a reduction peak at −0.49 V without a current plateau, indicating a $2e^-$ ORR process from O_2 to OOH^- under this voltage. In contrast, the wide current plateau on g-C_3N_4@CMK-3 is considered as the strong limiting diffusion current, indicating a diffusion-controlled process related to an efficient $4e^-$ dominated ORR pathway.

The durability of g-C_3N_4@CMK-3 is evaluated by the chronoamperometric response under a constant cathodic voltage of −0.3 V. As shown in Figure 3c, the newly developed catalyst exhibited high stability with a very slow attenuation after 45 h, and a high relative current of 92.2% still persisted. The CVs (inset in Figure 3c) also reveal the reliable stability of g-C_3N_4@CMK-3 with less than 10% cathodic current loss during ~10 000 continuous potential cyclings. This excellent stability benefits from homogeneous interactions of the g-C_3N_4 catalyst and CMK-3 support.

The methanol tolerance ability is an important issue for cathode materials in low-temperature fuel cells and also an obvious shortage of Pt-based catalysts. Remarkably, as shown in Figure 3d, the original cathodic ORR current of g-C_3N_4@CMK-3 under

−0.3 V did not show a significant change after the scheduled sequential addition of methanol into the electrolyte solution (the resulting methanol concentration is 3 M), suggesting that its original ORR performance was not affected by the addition of methanol. In comparison, the corresponding current on commercial Pt/C shifted from a cathodic current to a reversed anodic current in a very short time after the addition of methanol, indicating a conversion of the dominated oxygen reduction to the methanol oxidation reaction, i.e., a poisoning of the catalyst. RDE measurements carried out with/without methanol in the electrolyte solution further confirmed that g-C_3N_4@CMK-3 has a higher selectivity toward ORR to avoid crossover effects as compared to the commercial Pt/C catalyst (Figure S13). These results indicate that g-C_3N_4@CMK-3 is an ideal cathode catalyst for a direct methanol alkaline fuel cell.

A more detailed study of the RDE system at different rotating speeds was carried out to further investigate the electrode's electrocatalytic ORR mechanisms and dominated processes (Figure 3e). Calculated from the slope of the Koutecky−Levich plots (Figure 3f), the number of electrons transferred per O_2 molecule (n) for ORR is 2.6, 1.7, and 4.0 for g-C_3N_4(m), mixed g-C_3N_4+CMK-3, and g-C_3N_4@CMK-3, respectively. It is clear that the typical ORR process on g-C_3N_4(m) is a combined pathway of $2e^-$ and $4e^-$ reductions. In contrast, g-C_3N_4@CMK-3 shows perfect selectivity (nearly 100%) with a more efficient $4e^-$ dominated ORR process. To the best of our knowledge, this is the first report on metal-free electrocatalysts showing such excellent ORR catalytic efficiency. This efficiency is higher than that on other N-carbon materials including a nitrogen-doped carbon nanotube,[2b] nitrogen-doped graphitic carbon,[5d] nitrogen-doped mesoporous carbon,[8a] and nitrogen-doped grephene.[8d,e]

The n value on g-C_3N_4@CMK-3 is larger than that on Pt/C (n = 3.8, calculated from Figure S14), indicating its higher catalytic efficiency for ORR. Furthermore, the g-C_3N_4@CMK-3 reveals a calculated kinetic-limiting current density (J_k) value of 11.3 mA cm^{-2} at −0.6 V, much higher than those on g-C_3N_4(m) (1.7 mA cm^{-2}) and the mixed g-C_3N_4+CMK-3 (8.7 mA cm^{-2}), and comparable with that on Pt/C (11.3 mA cm^{-2}) at the same cathodic voltage and mass of catalyst (Figure S15). The large J_k value on g-C_3N_4@CMK-3 displays its excellent catalytic activity for ORR. The smaller n value and lower J_k on mixed g-C_3N_4+CMK-3 could be attributed to the poorer catalyst utilization due to its orderless structure and loose contact interface between the g-C_3N_4 catalyst and CMK-3 conductor. The variations in the kinetic Tafel plots for ORR further indicate the nanoconfinement phenomena involved in g-C_3N_4@CMK-3 facilitate faster ORR kinetics and lower diffusion limitations than those on mixed g-C_3N_4+CMK-3 (Figure S16). This alternative ORR mechanism and optimized ORR performance on g-C_3N_4@CMK-3 can be attributed to the participation of the CMK-3 mesoporous carbon framework, which not only serves as the support for the homogenously distributed and well-confined g-C_3N_4 catalyst but also significantly improves the electron accumulation on the surface of g-C_3N_4 catalyst, enhancing the ET efficiency in ORR.

In summary, on the basis of first-principle calculations, we designed and synthesized mesoporous g-C_3N_4@CMK-3 nanorods as a metal-free, facile-synthesis, and low-cost ORR electrocatalyst, which exhibited a competitive electrochemical performance with commercial Pt/C including extremely high electrocatalytic activity and efficiency. The excellent ORR performance and reliable stability of g-C_3N_4@CMK-3 indicate that this new catalyst is a promising candidate for the next generation of highly efficient ORR electrocatalysts particularly for methanol alkaline fuel cells. The results further open up new avenues for achieving a wide variety of cheap and commonly available metal-free catalysts for broad applications across the areas of heterogeneous catalysis, sensor, photonic catalysis, hydrogen production, and lithium ion batteries.

■ ASSOCIATED CONTENT

Supporting Information. Computational and experimental details, more characterization results, and detailed discussions. This material is available free of charge via the Internet at http://pubs.acs.org.

■ AUTHOR INFORMATION

Corresponding Author
s.qiao@uq.edu.au

■ ACKNOWLEDGMENT

This work was financially supported by the Australian Research Council (ARC) through the Discovery Project program (DP1095861, DP0987969). Y.J. acknowledges HPC time from AIBN cluster computing facility at UQ and ARC (LIEF Grant LE0882357).

■ REFERENCES

(1) (a) Steele, B. C. H.; Heinzel, A. *Nature* **2001**, *414*, 345. (b) Wu, G.; More, K. L.; Johnston, C. M.; Zelenay, P. *Science* **2011**, *332*, 443. (c) Gong, K.; Du, F.; Xia, Z.; Durstock, M.; Dai, L. *Science* **2009**, *323*, 760.

(2) (a) Matter, P. H.; Zhang, L.; Ozkan, U. S. *J. Catal.* **2006**, *239*, 83. (b) Tang, Y.; Allen, B. L.; Kauffman, D. R.; Star, A. *J. Am. Chem. Soc.* **2009**, *131*, 13200.

(3) Liu, Z.; Peng, F.; Wang, H.; Yu, H.; Zheng, W.; Yang, J. *Angew. Chem., Int. Ed.* **2011**, *50*, 3257.

(4) (a) Thomas, A.; Fischer, A.; Goettmann, F.; Antonietti, M.; Müller, J.; Schlögl, R.; Carlsson, J. M. *J. Mater. Chem.* **2008**, *18*, 4893. (b) Wang, X.; Maede, K.; Thomas, A.; Takanabe, K.; Xin, G.; Carsson, J. M.; Domen, K.; Antonietti, M. *Nat. Mater.* **2009**, *8*, 76. (c) Wang, Y.; Yao, J.; Li, H.; Su, D.; Antonietti, M. *J. Am. Chem. Soc.* **2011**, *133*, 2362. (d) Fischer, A.; Antonietti, M.; Thomas, A. *Adv. Mater.* **2007**, *19*, 264. (e) Zhang, Y.; More, T.; Ye, J.; Antonietti, M. *J. Am. Chem. Soc.* **2010**, *132*, 6294.

(5) (a) Lyth, S. M.; Nabae, Y.; Moriya, S.; Kuroki, S.; Kakimoto, M.; Ozaki, J.; Miyata, S. *J. Phys. Chem. C* **2009**, *113*, 20148. (b) Yang, S.; Feng, X.; Wang, X; Müllen, K. *Angew. Chem., Int. Ed.* **2011**, *50*, 5339. (c) Sun, Y.; Li, C.; Xu, Y.; Bai, H.; Yao, Z.; Shi, G. *Chem. Commun.* **2010**, *46*, 4740. (d) Liu, R.; Wu, D.; Feng, X.; Müllen, K. *Angew. Chem., Int. Ed.* **2010**, *49*, 2565.

(6) Tarasevich, M. R.; Sadkowski, A.; Yeager, E. *Comprehensive Treatise of Electrochemistry*, Vol. 7; Plenum: New York, 1983.

(7) (a) Ji, X.; Lee, K. T.; Nazar, L. F. *Nat. Mater.* **2009**, *8*, 500. (b) Jun, S.; Joo, S. H.; Ryoo, R.; Kruk, M.; Jaroniec, M.; Liu, Z.; Ohsuna, T.; Terasaki, O. *J. Am. Chem. Soc.* **2000**, *122*, 10712.

(8) (a) Yang, W.; Fellinger, T; Antonietti, M. *J. Am. Chem. Soc.* **2011**, *133*, 206. (b) Liu, R.; Malotki, C.; Arnold, L.; Koshino, N.; Higashimura, H.; Baumgarten, M.; Müllen, K. *J. Am. Chem. Soc.* **2011**, *133*, 10372. (c) Yang, L.; Jiang, S.; Zhao, Y.; Zhu, L.; Chen, S.; Wang, X.; Wu, Q.; Ma, J.; Ma, Y.; Hu, Z. *Angew. Chem., Int. Ed.* **2011**, *50*, 7132. (d) Geng, D.; Chen, Y.; Chen, Y.; Li, Y.; Li, R.; Sun, X.; Ye, S.; Knights, S. *Energy Environ. Sci.* **2011**, *4*, 760. (e) Sheng, Z.; Shao, L.; Chen, J.; Bao, W.; Wang, F.; Xia, X. *ACS Nano* **2011**, *5*, 4350.